XI International Conference on Computational Plasticity. Fundamentals and Applications
COMPLAS XI
E. Oñate, D.R.J. Owen, D. Peric and B. Suárez (Eds)

SHAPE OPTIMIZATION FOR ANISOTROPIC ELASTOPLASTICITY IN LOGARITHMIC STRAIN SPACE

S. GERMAIN* AND P. STEINMANN

Chair of Applied Mechanics
University of Erlangen-Nuremberg
Egerlandstr.5, 91058 Erlangen, Germany
www.ltm.uni-erlangen.de
*e-mail: sandrine.germain@ltm.uni-erlangen.de

Key words: Shape Optimization, Elastoplasticity, Anisotropy

Abstract. This paper deals with shape optimization for anisotropic elastoplasticity in logarithmic strain space. We aim to find an appropriate undeformed configuration of a workpiece knowing in advance its deformed configuration, the boundary conditions and the applied loads. The node coordinates of the finite element (FE) domain are chosen as design variables. A discrete sensitivity analysis is presented and analytical gradients are performed. A numerical example illustrates the theoretical aspects.

1 INTRODUCTION

A challenge in the design of functional parts is the determination of the initial, undeformed shape such that under a given load a part will obtain the desired deformed shape. This problem is inverse to the standard (direct) static analysis in which the undeformed shape is known and the deformed unknown. [1] extended the method originally proposed in [2] to anisotropic hyperelasticity that is based on logarithmic (Hencky) strains. [3] extended the method proposed in [1] to anisotropic elastoplastic materials. It was shown that the inverse form finding model in elastoplasticity can be used under the condition that the plastic strains are previously given. This is the case when a desired hardening state is prescribed. Basics on shape optimization can be found in [4]. In [5] a continuum sensitivity analysis is presented for the computation of shape sensitivity for finite hyperelastic-viscoplastic deformations. This method involves contact with friction using a direct differentiation method in 2D. [6] extented the work in [5] to thermoplasticity combined with ductile damage at finite strains. A gradient-based optimization framework for the computational design of metal forming processes for porous materials is introduced. [7] extented the work in [5] and [6] to 3D and defined the surface of the die by Bezier curves. This work focuses on the review of sensitivity contact. An alternative method

to continuum sensitivity analysis is a discrete formulation. This substitute has been applied in [8] for finite deformations in elastoplasticity in principal directions to parameter identification, which can be formulated as an optimization problem. [9] introduced a new regularization technique to avoid convergence problems and problems with jagged shapes. An artificial inequality constraint added to the optimization problems limits a fictitious total strain energy that measures the shape change of the design with respect to a reference design. The coordinates of boundary nodes of the FE-domain are chosen as design variables. The analytical gradients are derived using the adjoint method. The presented applications are restricted to linear elastostatic problems. [10, 11] proposed a shape optimization method for non-steady-state metal forming processes. The initial shape of a part as well as the shape of the preform tool during a two-step forging operation was optimized. Shapes are described using spline functions. The FE-method and remeshing operations are used during the simulation. Contact during the process are taken into account.
In this contribution we present a classical numerical shape optimization method for anisotropic elastoplastic materials that is based on logarithmic strains. A Limited–Broyden–Flechter–Goldfarb–Shanno (gradient-based descent method) algorithm from [12] is used. The objective function that needs to be minimized in order to obtain the optimal undeformed workpiece is the quadratic difference between the node positions in the targeted and computed deformed shape, i.e. the node coordinates of the FE-domain are chosen as design variables. A discrete sensitivity analysis is presented. Analytical gradients are performed. A remeshing of the shape is not applied during the computation.
This paper is organized as follows: In section 2 we briefly present the kinematics of the direct and the inverse problems. Section 3 summarizes anisotropic elastoplasticity in the logarithmic strain space. Section 4 presents the dissipation and the plastic flow response. In section 5 we review the Piola and Cauchy formulation to determine the deformed shape based on the knowledge of the undeformed shape. The finite element discretization is described in section 6. Section 7 presents the formulation of the sensitivity analysis. In section 8 a numerical example for the shape optimization in anisotropic elastoplasticity illustrates the theoritical aspects.

2 KINEMATICS OF GEOMETRICALLY NONLINEAR CONTINUUM MECHANICS

Let $\mathcal{B}_0$ denote the reference configuration of a continuum body with the boundary surface $\partial\mathcal{B}_0$ at time $t = 0$ parameterized by material coordinates $\boldsymbol{X}$. $\mathcal{B}_t$ is the current configuration with the boundary surface $\partial\mathcal{B}_t$ at time t parameterized by spatial coordinates $\boldsymbol{x}$, as depicted in Figure 1. The deformation map $\boldsymbol{\varphi}$ is defined as

$$\boldsymbol{x} = \boldsymbol{\varphi}(\boldsymbol{X}) : \mathcal{B}_0 \longrightarrow \mathcal{B}_t. \tag{1}$$

The corresponding deformation gradient together with its Jacobian determinant are given by

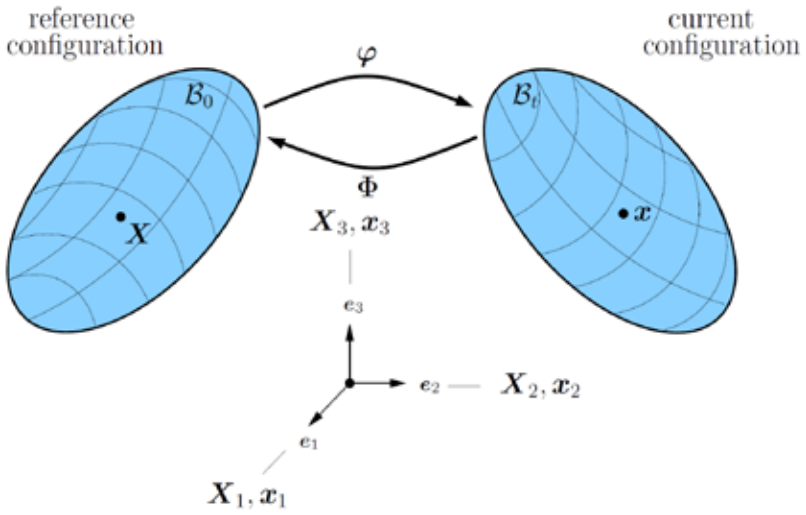

Figure 1: Nonlinear continuum mechanics.

$$\boldsymbol{F} = \nabla_{\boldsymbol{X}} \boldsymbol{\varphi}, \qquad J = \det \boldsymbol{F}. \tag{2}$$

$\nabla_{\boldsymbol{X}}$ denotes the gradient operator with respect to the material coordinates $\boldsymbol{X}$. The deformation map $\boldsymbol{\Phi}$ is defined as

$$\boldsymbol{X} = \boldsymbol{\Phi}(\boldsymbol{x}) : \mathcal{B}_t \longrightarrow \mathcal{B}_0. \tag{3}$$

The corresponding deformation gradient together with its Jacobian determinant are given by

$$\boldsymbol{f} = \nabla_{\boldsymbol{x}} \boldsymbol{\Phi}, \qquad j = \det \boldsymbol{f}. \tag{4}$$

$\nabla_{\boldsymbol{x}}$ denotes the gradient operator with respect to the spatial coordinates $\boldsymbol{x}$. It follows from the above definitions that

$$\boldsymbol{\Phi} = \boldsymbol{\varphi}^{-1}, \qquad \boldsymbol{f} = \boldsymbol{F}^{-1}, \qquad j = J^{-1}. \tag{5}$$

3 ANISOTROPIC ELASTOPLASTICITY IN LOGARITHMIC STRAIN SPACE

In this section we summarize the exposition in [13]. A valid model option for anisotropic finite strain elastoplasticity is a decomposition of the free energy into an elastic and a plastic part

$$\Psi = \psi^e + \psi^p. \tag{6}$$

The elastic part is a quadratic free energy density per unit volume in $\mathcal{B}_0$

$$\psi^e(\boldsymbol{E}^e) = \frac{1}{2}\boldsymbol{E}^e : \mathbb{E}^e : \boldsymbol{E}^e \tag{7}$$

in terms of the second-order elastic strain tensor $\boldsymbol{E}^e$ and a constant anisotropic elastic fourth-order stiffness tensor $\mathbb{E}^e$. For cubic materials, $\mathbb{E}^e$ can be decomposed into Kelvin modes [14] as

$$\mathbb{E}^e = 3\kappa\mathbb{P}_1 + 2\mu\mathbb{P}_2 + 2E_{55} \tag{8}$$

where κ is the bulk modulus, μ is the shear modulus and E_{55} is a constant material parameter. $\mathbb{P}_1$, $\mathbb{P}_2$ and $\mathbb{P}_3$ are fourth-order projection tensors. They can be expressed in terms of the volumetric and symmetric devatoric part of the fourth-order identity tensor as

$$\begin{aligned} \mathbb{P}_1 &= \mathbb{I}_{vol}, \\ \mathbb{P}_2 + \mathbb{P}_3 &= \mathbb{I}^{sym}_{dev}. \end{aligned} \tag{9}$$

An additive decomposition of the plastic strains into an elastic and a plastic part in terms of the second-order logarithmic (Hencky) strain tensor is assumed as

$$\boldsymbol{E} = \boldsymbol{E}^e + \boldsymbol{E}^p = \frac{1}{2}\ln \boldsymbol{C}. \tag{10}$$

Futhermore the plastic free energy part can be decomposed into parts which describe isotropic and kinematic hardening

$$\psi^p = \psi^{iso} + \psi^{kin}. \tag{11}$$

In the following only nonlinear isotropic hardening is considered. It follows

$$\psi^p = \psi^{iso} = \frac{1}{2}h\alpha + (\sigma_\infty - \sigma_0)(\alpha + \exp(\frac{-w\alpha}{w})) \tag{12}$$

where α is a scalar that models isotropic hardening. The spectral decomposition of the right Cauchy–Green strain tensor $\boldsymbol{C}$ reads

$$\boldsymbol{C} = \boldsymbol{F}^t \cdot \boldsymbol{F} = \sum_{i=1}^{3} \lambda_i \boldsymbol{M}_i \tag{13}$$

with $\{\lambda_i\}_{i=1,2,3}$ the real eigenvalues of $\boldsymbol{C}$ and $\{\boldsymbol{M}_i\}_{i=1,2,3}$ the associated eigenbases [15]. The spectral representation facilitates the computation of the logarithmic strain

$$\boldsymbol{E} = \frac{1}{2}\sum_{i=1}^{3} \ln \lambda_i \boldsymbol{M}_i \tag{14}$$

and allows a closed form expression for the (first and second) derivatives of the logarithmic strain with respect to the right Cauchy–Green strain

$$\mathbb{P} = 2\frac{\partial \boldsymbol{E}}{\partial \boldsymbol{C}} \quad \text{and} \quad \mathbb{L} = 2\frac{\partial \mathbb{P}}{\partial \boldsymbol{C}} = 4\frac{\partial^2 \boldsymbol{E}}{\partial \boldsymbol{C} \partial \boldsymbol{C}}. \tag{15}$$

For further details regarding the computation of these derivatives the interested reader is referred to [16]. Using (15), the Piola–Kirchhoff stress may be represented as

$$\boldsymbol{S} = 2\frac{\partial \Psi}{\partial \boldsymbol{C}} = \boldsymbol{T} : \mathbb{P} \quad \text{with} \quad \boldsymbol{T} = \frac{\partial \Psi}{\partial \boldsymbol{E}^e} = \mathbb{E}^e : \boldsymbol{E}^e. \tag{16}$$

Considering this expression, the linearization of the Piola–Kirchhoff stress (tangent operator needed in a Newton type solution scheme) reads

$$\mathbb{C} = 4\frac{\partial^2 \Psi}{\partial \boldsymbol{C} \partial \boldsymbol{C}} = \mathbb{P}^T : \mathbb{E}^* : \mathbb{P} + \boldsymbol{T} : \mathbb{L} \quad \text{with} \quad \mathbb{E}^* = \frac{\partial^2 \Psi}{\partial \boldsymbol{E} \partial \boldsymbol{E}}. \tag{17}$$

The transposition symbol $[\bullet]^T$ refers to an exchange of the first and last pairs of indices. The fourth-order tensor $\mathbb{E}^*$ is the fourth-order elasticity tensor $\mathbb{E}^e$ in the case of an elastic loading and the elastoplasticity tensor $\mathbb{E}^{ep}$ in the case of a plastic loading [13], respectively.

4 DISSIPATION AND PLASTIC FLOW RESPONSE

In the logarithmic strain space the dissipation inequality can be written as

$$\boldsymbol{T} : \overset{\circ}{\boldsymbol{E}}{}^p - \frac{\partial \Psi}{\partial \alpha} \cdot \overset{\circ}{\alpha} \geq 0, \tag{18}$$

where $[\overset{\circ}{\bullet}]$ denotes the time derivative and $\{\boldsymbol{E}^p, \alpha\}$ is the set of internal variables. We consider the following quadratic yield function

$$\Upsilon = \|\mathrm{dev}\boldsymbol{T}\| - \sqrt{\frac{2}{3}} B \quad \text{with} \quad B = h\alpha + (\sigma_\infty - \sigma_0)(1 - \exp(-w\alpha)). \tag{19}$$

Using the principle of maximum plastic dissipation and the definition of the Lagrange function $\mathcal{L}$,

$$\mathcal{L}(\boldsymbol{T}, \frac{\partial \Psi}{\partial \alpha}, \gamma) = -\boldsymbol{T} : \overset{\circ}{\boldsymbol{E}}{}^p - \frac{\partial \Psi}{\partial \alpha} \cdot \overset{\circ}{\alpha} + \gamma(\Upsilon - \sqrt{\frac{2}{3}}\sigma_0), \tag{20}$$

we obtain the Karush-Kuhn-Tucker equations

$$\left\{ \begin{array}{c} \overset{\circ}{\boldsymbol{E}}{}^p = \gamma \dfrac{\partial \Upsilon}{\partial \boldsymbol{T}}, \quad \overset{\circ}{\alpha} = \gamma \dfrac{\partial \Upsilon}{\partial B} = \sqrt{\dfrac{2}{3}}\gamma, \\ \gamma \geq 0, \quad \Upsilon - \sqrt{\dfrac{2}{3}}\sigma_0 \leq 0 \quad \text{and} \quad \gamma\Upsilon = 0, \end{array} \right. \tag{21}$$

where $\gamma \geq 0$.

5 DETERMINING THE DEFORMED SHAPE FROM EQUILIBRIUM

In this contribution we omit distributed body forces and inertia henceforth.

5.1 Piola formulation

The Piola formulation for the equilibrium is determined by the following boundary value problem

$$\begin{aligned} \mathrm{Div}\boldsymbol{P} &= \boldsymbol{0} \quad \text{in} \quad \mathcal{B}_0, \\ [\boldsymbol{F}\cdot\boldsymbol{S}]\cdot\boldsymbol{N} &= \boldsymbol{t}_0 \quad \text{on} \quad \partial\mathcal{B}_0^t, \\ \boldsymbol{\varphi} &= \overline{\boldsymbol{\varphi}} \quad \text{on} \quad \partial\mathcal{B}_0^{\varphi} \end{aligned} \tag{22}$$

where $\partial\mathcal{B}_0^t$ corresponds to the part of the boundary surface where the Direchlet boundary conditions hold, $\partial\mathcal{B}_0^{\varphi}$ corresponds to the part of the boundary surface where the Neumann boundary conditions hold and we set

$$\partial\mathcal{B}_0 = \mathcal{B}_0^t \bigcup \mathcal{B}_0^{\varphi} \quad \text{with} \quad \mathcal{B}_0^t \bigcap \mathcal{B}_0^{\varphi} = \varnothing. \tag{23}$$

$\boldsymbol{N}$ is defined as a unit vector at $\boldsymbol{X}$ directed along the outward normal to an material surface element $\mathrm{d}A \in \partial\mathcal{B}_0^t$. $\boldsymbol{t}_0$ is the first Piola-Kirchhoff traction vector exerted on $\mathrm{d}A$ with normal $\boldsymbol{N}$. Div denotes the material divergence operator with respect to the material coordinates $\boldsymbol{X}$. Accordingly, the weak form of the given boundary value problem reads, with the test function $\boldsymbol{\eta} = \boldsymbol{0}$ on the boundary surface $\partial\mathcal{B}_0^{\varphi}$,

$$G(\boldsymbol{\varphi}, \boldsymbol{\eta}; \boldsymbol{X}) = \int_{\mathcal{B}_0} [\boldsymbol{F}^t \cdot \nabla_{\boldsymbol{X}}\boldsymbol{\eta}] : \boldsymbol{S}\,\mathrm{d}V - \int_{\partial\mathcal{B}_0} \boldsymbol{\eta}\cdot\boldsymbol{t}_0\,\mathrm{d}A = 0. \tag{24}$$

The above expression is the common virtual work statement with a parameterization of all quantities in the material coordinates $\boldsymbol{X}$. The (symmetric) Piola–Kirchhoff stress is expressed as a functional of $\boldsymbol{\varphi} = \boldsymbol{\varphi}(\boldsymbol{X})$ as

$$\boldsymbol{S} = \boldsymbol{S}(\nabla_{\boldsymbol{X}}\boldsymbol{\varphi}(\boldsymbol{X})). \tag{25}$$

The corresponding linearization (directional derivative) of the weak form in the direction $\Delta\boldsymbol{\varphi}$ at fixed material coordinates $\boldsymbol{X}$, as needed in a Newton type solution scheme, is finally expressed as

$$\frac{d}{d\epsilon} G(\boldsymbol{\varphi} + \epsilon\Delta\boldsymbol{\varphi}, \boldsymbol{\eta}; \boldsymbol{X})|_{\epsilon=0} = \int_{\mathcal{B}_0} \nabla_{\boldsymbol{X}}\boldsymbol{\eta} : \mathbb{A} : \Delta\boldsymbol{F}\,\mathrm{d}V. \tag{26}$$

The fourth-order tangent operator $\mathbb{A}$ decomposes into the material tangent operator $\mathbb{C}$ (see (17)) and a geometrical contribution

$$\mathbb{A} := \frac{\partial[\boldsymbol{F}\cdot\boldsymbol{S}]}{\partial\boldsymbol{F}} = [\boldsymbol{F}\overline{\otimes}\boldsymbol{I}] : \mathbb{C} : [\boldsymbol{F}^t\overline{\otimes}\boldsymbol{I}] + \boldsymbol{i}\overline{\otimes}\boldsymbol{S}. \tag{27}$$

In the above expression $\boldsymbol{I}$ and $\boldsymbol{i}$ denote the material and spatial unit tensors with coefficients δ_{IJ} and δ_{ij}, respectively, $\overline{\otimes}$ denotes a non-standard dyadic product with $[\boldsymbol{A}\overline{\otimes}\boldsymbol{B}]_{IJKL} = A_{IK}B_{JL}$ and $I, J, K, L, i, j = 1\ldots3$.

5.2 Cauchy stress formulation

The equilibrium statement may alternatively be expressed by the following variant of the boundary value problem (Cauchy stress formulation) in terms of spatial description quantities

$$\begin{aligned} \operatorname{div}\boldsymbol{\sigma} &= \mathbf{0} \quad \text{in} \quad \mathcal{B}_t, \\ \boldsymbol{\sigma}\cdot\boldsymbol{n} &= \boldsymbol{t} \quad \text{on} \quad \partial\mathcal{B}_t^t, \\ \boldsymbol{\varphi} &= \overline{\boldsymbol{\varphi}} \quad \text{on} \quad \partial\mathcal{B}_t^{\varphi} \end{aligned} \tag{28}$$

where $\partial\mathcal{B}_t^t$ corresponds to the part of the boundary surface where the Direchlet boundary conditions hold, $\partial\mathcal{B}_t^{\varphi}$ corresponds to the part of the boundary surface where the Neumann boundary conditions hold and we set

$$\partial\mathcal{B}_t = \mathcal{B}_t^t \bigcup \mathcal{B}_t^{\varphi} \quad \text{with} \quad \mathcal{B}_t^t \bigcap \mathcal{B}_t^{\varphi} = \varnothing. \tag{29}$$

div denotes the divergence operator with respect to the spatial coordinates $\boldsymbol{x}$. $\boldsymbol{n}$ is defined as a unit vector at $\boldsymbol{x}$ directed along the outward normal to an spatial surface element $\mathrm{d}a \in \partial\mathcal{B}_t$ and $\boldsymbol{t}$ represents the Cauchy traction vector exerted on $\mathrm{d}a$ with normal $\boldsymbol{n}$. The (symmetric) Cauchy stress $\boldsymbol{\sigma}$ is obtained from the Piola–Kirchhoff stress by a push-forward according to

$$J\boldsymbol{\sigma} = \boldsymbol{F}\cdot\boldsymbol{S}\cdot\boldsymbol{F}^t. \tag{30}$$

Accordingly, the weak form of the given boundary value problem, corresponding to the equilibrium requirement for the spatial configuration, reads with the test function $\boldsymbol{\eta} = \mathbf{0}$ on the boundary surface $\partial\mathcal{B}_t^{\varphi}$

$$g(\boldsymbol{\Phi}, \boldsymbol{\eta}; \boldsymbol{x}) = \int_{\mathcal{B}_t} \nabla_{\boldsymbol{x}}\boldsymbol{\eta} : \boldsymbol{\sigma}\, \mathrm{d}v - \int_{\partial\mathcal{B}_t^t} \boldsymbol{\eta}\cdot\boldsymbol{t}\, \mathrm{d}a = 0. \tag{31}$$

The corresponding linearization (directional derivative) of the weak form in the direction $\Delta\boldsymbol{\Phi}$ at fixed spatial coordinates $\boldsymbol{x}$, as needed in a Newton type solution scheme, is finally expressed as

$$\frac{d}{d\epsilon} g(\boldsymbol{\Phi} + \epsilon\Delta\boldsymbol{\Phi}, \boldsymbol{\eta}; \boldsymbol{x})|_{\epsilon=0} = \int_{\mathcal{B}_t} \nabla_{\boldsymbol{x}}\boldsymbol{\eta} : \mathbb{a} : \Delta\boldsymbol{f}\, \mathrm{d}v. \tag{32}$$

The fourth-order tangent operator $\mathbb{a}$ is depicted as

$$\mathbb{a} := \frac{\partial[j\boldsymbol{F}\cdot\boldsymbol{S}\cdot\boldsymbol{F}^t]}{\partial\boldsymbol{f}} = \boldsymbol{\sigma}\otimes\boldsymbol{F}^t - \boldsymbol{F}\overline{\otimes}\boldsymbol{\sigma} + j\boldsymbol{F}\cdot\left[\frac{1}{2}\mathbb{C} : \frac{\partial\boldsymbol{C}}{\partial\boldsymbol{f}}\right]\cdot\boldsymbol{F}^t - \boldsymbol{\sigma}\underline{\otimes}\boldsymbol{F}. \tag{33}$$

The derivative of the right Cauchy–Green strain is expressed as

$$\frac{\partial\boldsymbol{C}}{\partial\boldsymbol{f}} = -\boldsymbol{F}^t\underline{\otimes}\boldsymbol{C} - \boldsymbol{C}\overline{\otimes}\boldsymbol{F}^t. \tag{34}$$

In the above equations, the non-standard dyadic product $\underline{\otimes}$ is defined by $[\boldsymbol{A}\underline{\otimes}\boldsymbol{B}]_{IJKL} = A_{IL}B_{JK}$ and $I, J, K, L = 1\ldots 3$.

6 DISCRETIZATION

For the finite element solution of the two problems ((24) and (31)) the material solution domain $\mathcal{B}_0$ is discretized into n_{el} elements

$$\mathcal{B}_0 \approx \mathcal{B}_0^h = \bigcup_{e=1}^{n_{el}} \mathcal{B}_0^e. \tag{35}$$

Following the standard isoparametric approach, the geometry is approximated on each element by the following shape functions

$$\boldsymbol{X}^e(\boldsymbol{\xi}) = \sum_{i=1}^{n_{en}} \boldsymbol{X}^{(i)} N^{(i)}(\boldsymbol{\xi}), \qquad \boldsymbol{x}^e(\boldsymbol{\xi}) = \sum_{i=1}^{n_{en}} \boldsymbol{x}^{(i)} N^{(i)}(\boldsymbol{\xi}). \tag{36}$$

Thereby the shape functions $N^{(i)}$ are parameterized by isoparametric coordinates $\boldsymbol{\xi}$ defined on the isoparametric cube $\mathcal{B}^\xi = [-1, 1]^3$, whereas n_{en} is the total number of nodes per element, and $\boldsymbol{X}^{(i)}$ and $\boldsymbol{x}^{(i)}$ denote nodal values. Finally, following the Bubnov–Galerkin method the test function is again approximated by the same shape functions $N^{(i)}$

$$\boldsymbol{\eta}^e(\boldsymbol{\xi}) = \sum_{i=1}^{n_{en}} \boldsymbol{\eta}^{(i)} N^{(i)}(\boldsymbol{\xi}). \tag{37}$$

Substituting the finite element approximations into the weak form, we obtain the discrete equilibrium condition as a residual that is expressed at each node (i) (n_{np} is the total number of node points) as

$$\boldsymbol{r}^{(i)} = \boldsymbol{r}^{(i)}_{ext} - \boldsymbol{r}^{(i)}_{int} \qquad \text{with} \qquad i = 1 \dots n_{np}. \tag{38}$$

The contributions to the internal and external nodal forces read

$$\begin{aligned} \boldsymbol{r}^{(i)}_{int} &= \mathop{\mathsf{A}}_{e=1}^{n_{el}} \int_{\mathcal{B}_0^e} [\boldsymbol{F} \cdot \boldsymbol{S}] \cdot \nabla_{\boldsymbol{X}} N^{(i)} \, \mathrm{d}V = \mathop{\mathsf{A}}_{e=1}^{n_{el}} \int_{\mathcal{B}_t^e} \boldsymbol{\sigma} \cdot \nabla_{\boldsymbol{x}} N^{(i)} \, \mathrm{d}v, \\ \boldsymbol{r}^{(i)}_{ext} &= \mathop{\mathsf{A}}_{e=1}^{n_{el}} \int_{\partial\mathcal{B}_0^{e,t}} \boldsymbol{t}_0^e N^{(i)} \, \mathrm{d}A = \mathop{\mathsf{A}}_{e=1}^{n_{el}} \int_{\partial\mathcal{B}_t^{e,t}} \boldsymbol{t}_t^e N^{(i)} \, \mathrm{d}a. \end{aligned} \tag{39}$$

The tangent stiffness matrix $\boldsymbol{k}$ is defined as the Jacobian matrix of the residual (Piola formulation) with respect to the spatial coordinates as

$$\boldsymbol{k}^{(ij)} := -\frac{\partial \boldsymbol{r}^{(i)}}{\partial \boldsymbol{x}^{(j)}} = \mathop{\mathsf{A}}_{e=1}^{n_{el}} \int_{\mathcal{B}_0^e} \nabla_{\boldsymbol{X}} N^{(i)} \overset{2}{\cdot} \mathbb{A} \cdot \nabla_{\boldsymbol{X}} N^{(j)} \, \mathrm{d}V. \tag{40}$$

The tangent stiffness matrix $\boldsymbol{K}$ is defined as the Jacobian matrix of the residual (Cauchy stress formulation) with respect to the material coordinates as

$$\boldsymbol{K}^{(ij)} := -\frac{\partial \boldsymbol{r}^{(i)}}{\partial \boldsymbol{X}^{(j)}} = \mathop{\mathsf{A}}_{e=1}^{n_{el}} \int_{\mathcal{B}_t^e} \nabla_{\boldsymbol{x}} N^{(i)} \overset{2}{\cdot} \mathfrak{a} \cdot \nabla_{\boldsymbol{x}} N^{(j)} \, \mathrm{d}v. \tag{41}$$

In the above expressions $\overset{2}{\cdot}$ denotes contraction with the second index of the corresponding tangent operator.

7 SENSITIVITY ANALYSIS

The aim of the sensitivity analysis is to supply the gradients of the objective function and the constraints with respect to the design variables, which are necessary for the use of gradient-based optimization algorithms [9]. In the following we restrict ourself to unconstraint problems. The objective function is defined as

$$f(\boldsymbol{X}) = \frac{1}{2}[\boldsymbol{x}^{\text{target}} - \boldsymbol{x}^{\text{current}}(\boldsymbol{X})]^2 \rightarrow \min_{\boldsymbol{X}} \tag{42}$$

where the material coordinates $\boldsymbol{X}$ are the design variables. By applying the chain rule, we obtain

$$\frac{\mathrm{d}f(\boldsymbol{X})}{\mathrm{d}\boldsymbol{X}} = \frac{\partial f^{\text{explicite}}}{\partial \boldsymbol{X}} + \frac{\partial f}{\partial \boldsymbol{x}^{\text{current}}} \frac{\mathrm{d}\boldsymbol{x}^{\text{current}}}{\mathrm{d}\boldsymbol{X}}. \tag{43}$$

According to the implicite dependency of the objective function to $\boldsymbol{X}$ we have

$$\frac{\partial f^{\text{explicite}}}{\partial \boldsymbol{X}} = 0 \qquad \text{and then} \qquad \frac{\mathrm{d}f(\boldsymbol{X})}{\mathrm{d}\boldsymbol{X}} = \frac{\partial f}{\partial \boldsymbol{x}^{\text{current}}} \frac{\mathrm{d}\boldsymbol{x}^{\text{current}}}{\mathrm{d}\boldsymbol{X}}. \tag{44}$$

The key for the computation of the Jacobian matrix $\dfrac{\mathrm{d}\boldsymbol{x}^{\text{current}}}{\mathrm{d}\boldsymbol{X}}$ in (44) is the mechanical equilibrium condition [9]

$$\boldsymbol{r}^{\text{current}}(\boldsymbol{X}) = \boldsymbol{r}(\boldsymbol{x}^{\text{current}}(\boldsymbol{X}), \boldsymbol{X}) = \boldsymbol{r}_{ext} - \boldsymbol{r}_{int}(\boldsymbol{x}^{\text{current}}(\boldsymbol{X}), \boldsymbol{X}) = 0. \tag{45}$$

Applying the total differential on the above equation we obtain

$$\frac{\mathrm{d}\boldsymbol{r}^{\text{current}}}{\mathrm{d}\boldsymbol{X}} = \frac{\partial \boldsymbol{r}}{\partial \boldsymbol{X}} + \frac{\partial \boldsymbol{r}}{\partial \boldsymbol{x}^{\text{current}}} \frac{\mathrm{d}\boldsymbol{x}^{\text{current}}}{\mathrm{d}\boldsymbol{X}} = 0. \tag{46}$$

After a rearrangement we deduce

$$\frac{\mathrm{d}\boldsymbol{x}^{\text{current}}}{\mathrm{d}\boldsymbol{X}} = -[\frac{\partial \boldsymbol{r}}{\partial \boldsymbol{x}^{\text{current}}}]^{-1} \frac{\partial \boldsymbol{r}}{\partial \boldsymbol{X}}. \tag{47}$$

Substituting (47) in (44) we obtain

$$\frac{\mathrm{d}f(\boldsymbol{X})}{\mathrm{d}\boldsymbol{X}} = -\frac{\partial f}{\partial \boldsymbol{x}^{\text{current}}}[\frac{\partial \boldsymbol{r}}{\partial \boldsymbol{x}^{\text{current}}}]^{-1} \frac{\partial \boldsymbol{r}}{\partial \boldsymbol{X}} = (\boldsymbol{x}^{\text{target}} - \boldsymbol{x}^{\text{current}})[\frac{\partial \boldsymbol{r}}{\partial \boldsymbol{x}^{\text{current}}}]^{-1} \frac{\partial \boldsymbol{r}}{\partial \boldsymbol{X}}. \tag{48}$$

Considering the form of (40) and (41) we finally obtain

$$\frac{\mathrm{d}f(\boldsymbol{X})}{\mathrm{d}\boldsymbol{X}} = (\boldsymbol{x}^{\text{target}} - \boldsymbol{x}^{\text{current}})[\boldsymbol{k}]^{-1}\boldsymbol{K}.$$

8 NUMERICAL EXAMPLE

As an example we simulate a tension test on a cylinder with an internal hole in 3D. The outer diameter of the cylinder is 20mm, the inner diameter is 10mm and the thickness is 30mm. The base of the cylinder is clamped (red squares on Figure 3). A distributed load F=110kN is applied on the top of the cylinder (red arrows on Figure 3). We consider an anisotropic elastoplastic material with a cubic symmetry and the following properties: E=210000MPa, μ=0.3, E_{55}=60000MPa, h=305MPa, σ_0=180MPa, σ_∞=305MPa and w=15. The domain is discretized using trilinear hexahedral finite elements (50 elements and 120 nodes). Figure 2 shows the deformed shape on which the obtained von Mises stresses are plotted after applying loads and boundary conditions on the computed undeformed sheet (Figure 3). As expected the top outer diameter of the computed undeformed cylinder (Figure 3) became larger and the thickness of the undeformed cylinder has been reduced. The convergence time to the solution is 4 hours 49 min 32s. The L-BFGS algorithm needs 23 iterations to find a minimum less than 10^{-14}.

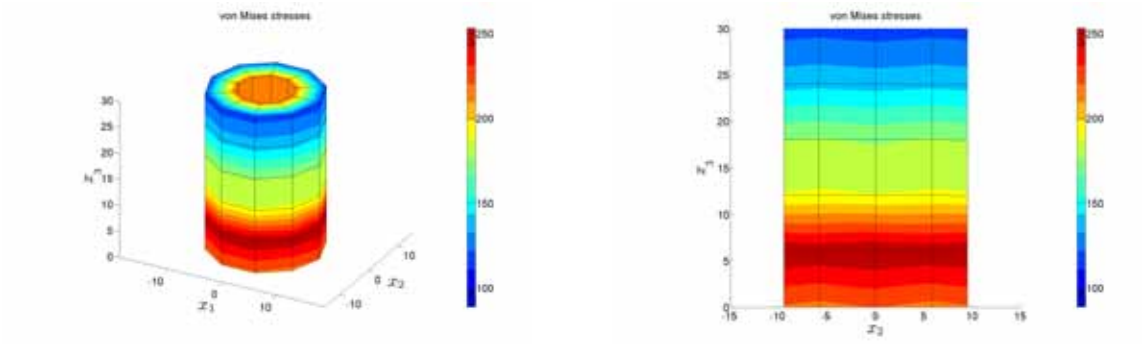

Figure 2: Deformed sheet with von Mises stresses in the final configuration $\mathcal{B}_t$.

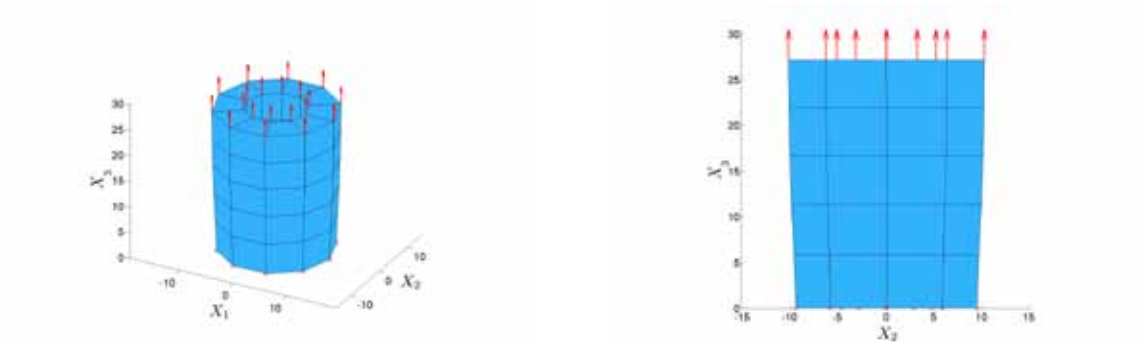

Figure 3: Undeformed sheet in the reference configuration $\mathcal{B}_0$.

9 CONCLUSION

This work presents a three dimensional procedure for anisotropic elastoplastic materials based on shape optimization theory. The aim is the determination of the undeformed shape of a workpiece when knowing its desired deformed shape, the boundary conditions and the loads. A logarithmic strain space formulation is used. A spectral decomposition of the right Cauchy–Green tensor allows a simple evaluation and linearization of the logarithmic strain measure. The node coordinates of the finite element domain, excluding the boundary conditions, are chosen as design variables. The gradient of the objective function needed by the L-BFGS algorithm is computed analytically using a discrete sensitivity analysis approach. A numerical example in nonlinear cubic elastoplasticity illustrates the ability to numerically approximate the undeformed shape. Future research will be conducted on the remeshing of the workpiece during the computation and a regularization will be considered in order to avoid mesh distorsions.

ACKNOWLEDGEMENT

This work was supported by the German Research Foundation (DFG) under the Transregional Collaborative Research Center SFB/TR73: "Manufacturing of Complex Functional Components with Variants by Using a New Sheet Metal Forming Process - Sheet-Bulk Metal Forming".

REFERENCES

[1] S. Germain, M. Scherer and P. Steinmann, *On Inverse Form Finding for Anisotropic Hyperelasticity in Logarithmic Strain Space*. Int. J. of Structural Changes in Solids - Mechanics and Applications, Vol. 2. No.2, pp.1–16 (November 2010).

[2] S. Govindjee and P.A. Mihalic, *Computational methods for inverse finite elastostatics*, Comput. Methods Appl. Mech. Engrg., Vol. 136, pp.47–57 (1996).

[3] S. Germain and P. Steinmann, *On Inverse Form Finding for Anisotropic Elastoplastic Materials*, The 14th International ESAFORM Conference on Material Forming, AIP Conf. Proc., Vol. 1353, pp.1169–1174 (2011).

[4] D.G. Luenberger, *Linear and nonlinear programming*, Addison-Wesley Publishing Company, Second Edition (1984).

[5] A. Srikanth and N. Zabaras, *Shape optimization and preform design in metal forming processes*, Comput. Methods Appl. Mech. Engrg., Vol. 190, pp.1859–1901 (2000).

[6] S. Ganapathysubramanian and N. Zabaras, *Computational design of deformation processes for materials with ductile damage*, Comput. Methods Appl. Mech. Engrg., Vol. 192, pp.147–183 (2003).

[7] S. Acharjee and N. Zabaras, *The continuum sensitivity method for computational design of three-dimensional deformation processes*, Comput. Methods Appl. Mech. Engrg., Vol. 195, pp.6822–6842 (2006).

[8] R. Mahnken and E. Stein, *A unified approach for parameter identification of inelastic material models in the frame of the finite element method*, Comput. Methods. Appl. Mech. Engrg., Vol.136, pp.225-258 (1996).

[9] M. Scherer, R. Denzer and P. Steinmann, *A fictitious energy approach for shape optimization*, Int. J. Numer. Meth. Engng., Vol. 82, pp.269–302 (2010).

[10] L. Fourment and J. L. Chenot, *Optimal design for non-steady-state metal forming processes - I. Shape optimization method*, Int. J. Numer. Meth. Engng., Vol. 39, pp.33–50 (1996).

[11] L. Fourment and J. L. Chenot, *Optimal design for non-steady-state metal forming processes - II. Application of shape optimization in forging*, Int. J. Numer. Meth. Engng., Vol. 39, pp.51–65 (1996).

[12] M. Schmidt, http://www.cs.ubc.ca/schmidtm/Software/minFunc.html (2005).

[13] N. Apel, *Approaches to the Description of Anisotropic Material Behaviour at Finite Elastic and Plastic Deformations - Theory and Numerics*, In: Prof. Dr.-Ing. C. Miehe (Hrsg.): Institut fuer Mechanik (Bauwesen), Lehrsthul I, Universitaet Stuttgart, Dissertation, Bericht Nr.: I-12 (2004).

[14] S. Sutcliffe, *Spectral Decomposition of the Elasticity Tensor*, J. of Applied Mechanics, Vol. 59, 1992, pp.762–773 (1992).

[15] C. Miehe, *Computation of isotropic tensor functions*, Communications in numerical methods in engineering, Vol. 9, pp.889–896 (1993).

[16] C. Miehe and M. Lambrecht, *Algorithms for computation of stresses and elasticity moduli in terms of Seth-Hill's family of generalized strain tensors*, Communications in numerical methods in engineering, Vol. 17, pp.337–353 (2001).